An embedded network approach for scale-up of fluctuation-driven systems with preservation of spike information

David Cai*†, Louis Tao‡, and David W. McLaughlin*§

*Courant Institute of Mathematical Sciences and §Center for Neural Science, New York University, New York, NY 10012; and ‡Department of Mathematical Sciences, New Jersey Institute of Technology, Newark, NJ 07102

Contributed by David W. McLaughlin, June 8, 2004

To address computational "scale-up" issues in modeling large regions of the cortex, many coarse-graining procedures have been invoked to obtain effective descriptions of neuronal network dynamics. However, because of local averaging in space and time, these methods do not contain detailed spike information and, thus, cannot be used to investigate, e.g., cortical mechanisms that are encoded through detailed spike-timing statistics. To retain high-order statistical information of spikes, we develop a hybrid theoretical framework that embeds a subnetwork of point neurons within, and fully interacting with, a coarse-grained network of dynamical background. We use a newly developed kinetic theory for the description of the coarse-grained background, in combination with a Poisson spike reconstruction procedure to ensure that our method applies to the fluctuation-driven regime as well as to the mean-driven regime. This embedded-network approach is verified to be dynamically accurate and numerically efficient. As an example, we use this embedded representation to construct "reverse-time correlations" as spiked-triggered averages in a ring model of orientation-tuning dynamics.

Many levels of neuronal representations have been developed in modeling regions of the cortex. Good representations can provide powerful theoretical insights into the workings of the brain and increase significantly our understanding of fundamental cortical mechanisms. However, in computational modeling efforts one immediately confronts crucial issues of "scale-up" to model sufficiently large regions of the cortex; for example, to investigate real-world perception and optical illusions in visual cortex. These scale-up issues have been addressed through a hierarchy of reduction and "coarse-graining" steps: simplifying multicompartment neuron models to fewer compartment models, replacing point neuron representations with more coarse-grained (CG) representations that deal only with spatially/temporally local-averaged quantities, such as mean firing rate (1–3) and population density representations (4–12). Because of local time averaging, detailed information about spikes, such as interspike interval (ISI) distributions, is lost in these CG approaches, including the kinetic theory (12) (which still invokes CG in time despite its success in describing fluctuation effects). Thus, cortical mechanisms that are encoded through detailed spike-timing statistical patterns cannot be investigated with the present CG techniques.

Here, we introduce a *hybrid framework*, which retains detailed, high-order statistical information of spikes, yet is numerically efficient and effective for scale-up. The hybridization is accomplished by embedding a subnetwork of point neurons within a CG substrate or background network. This approach is designed to address situations where a biologically distinct subnetwork of neurons interacts with the remaining neuronal population of the substrate. For example, local interactions between point neurons might be represented as a background by local averages in space and time, whereas sparse (but sufficiently strong) long-range interactions would be represented by a subnetwork of the embedded point neurons. Alternatively, a special class of cells might have particularly strong sparse connections, such as those connecting different cortical layers. Or neurons within special cortical regions, such as near orientation pinwheel centers where interaction strengths change so rapidly over short cortical distances that local spatial averaging is not valid, might necessitate the use of embedded neurons. In our approach, we ensure that these two networks (the CG background and the embedded point neurons) can fully interact, with each influencing the other. Because they are fully interacting with the CG background, conceptually, these embedded point neurons differ from the notion of "test particles" familiar in physics. Naturally, if the couplings of the embedded network are very sparse and weak, then the embedded neurons reduce to "test neurons" for extracting information about the background.

In the hybrid approach, the level of detail required in modeling specific neuronal phenomena dictates the specification of particular representations for each of the two networks. For example, for the embedded point neurons, we might invoke an integrate-and-fire (I&F) model, or a more realistic one, such as a Hodgkin–Huxley model. For the CG background, we could use a dynamics of mean firing rates or population density. In this work, we use a leaky I&F description for the embedded point neurons; for the CG background, the kinetic theory (12) that we recently developed to capture fluctuation-dominated network dynamics. We choose this kinetic representation specifically to emphasize that the embedded network method has wide applicability, even for regimes which are driven by fluctuations.

In what follows, this *embedded* representation is developed and its performance is evaluated; its accuracy, efficiency, and numerical effectiveness are established through simulations in comparison with the original I&F networks. We also contrast the kinetic representation with simpler "mean firing rate" representations of the background, demonstrating that, in fluctuation-driven regimes, the kinetic theory provides a far more accurate description of the original dynamics than the mean firing rate. We also use the embedded representation to simulate "reverse time correlation" (RTC) experiments, which, as spike triggered averages, provide one example in which the retention of spike-timing information is natural. Finally, we discuss future generalizations and possible applications.

Methods

We first coarse-grain a layer of cortex into many, small CG patches as described in refs. 2 and 12. As a specific example, we take one small CG patch from our large-scale numerical model (13–15) of the input layer $4C\alpha$ of primary visual cortex (V1) of the macaque monkey, which consists of 75% excitatory and 25% inhibitory cells of both simple and complex types, represented as

Abbreviations: CG, coarse-grained; ISI, interspike interval; I&F, integrate-and-fire; RTC, reverse time correlation; PSR, Poisson spike reconstruction.

†To whom correspondence should be addressed. E-mail: cai@cims.nyu.edu.

www.pnas.org/cgi/doi/10.1073/pnas.0404062101

I&F point neurons. In ref. 12 we described an asymptotic reduction of this large-scale point-neuron network to a CG kinetic representation that is well suited for scale-up. We showed that this kinetic theory is dynamically accurate and numerically efficient, even when the original point-neuron network is fluctuation-dominant. However, the coarse-graining procedure in the derivation of the kinetic theory includes a local average over time, thus removing detailed spike-timing information. Here, to regain this spike information, we take the hybrid approach, identifying a distinguished subnetwork of point neurons that will be retained and replacing the other neurons with a CG kinetic description.

Now, we turn to the description of the essential steps used in this hybridization procedure. Partition the original network into two subpopulations, a "minority" population comprising the distinguished subnetwork of embedded neurons and a "majority" population that is to be coarse-grained and constitutes a CG background patch. The ith neuron in this majority population satisfies the I&F dynamics,

$$\tau \frac{d}{dt} V_{\alpha i}^{\lambda} = -(V_{\alpha i}^{\lambda} - V_R) - G_{\alpha i}^{\lambda E}(t)(V_{\alpha i}^{\lambda} - V_E) - G_{\alpha i}^{\lambda I}(t)(V_{\alpha i}^{\lambda} - V_I), \quad [1a]$$

$$\sigma_{\lambda'} \frac{d}{dt} G_{\alpha i}^{\lambda\lambda'} = -G_{\alpha i}^{\lambda\lambda'} + \eta_{\alpha i}^{\lambda\lambda'} + \xi_{\alpha i}^{\lambda\lambda'} + \gamma_{\alpha BD}^{\lambda\lambda'}, \quad [1b]$$

together with the spike-to-reset dynamics. Here, $\eta_{\alpha i}^{\lambda\lambda'}$ describes the external drive, $\xi_{\alpha i}^{\lambda\lambda'}$ describes the cortico-cortical couplings among neurons in the CG background, and $\gamma_{\alpha BD}^{\lambda\lambda'}$ describes the feedback from the remaining, embedded neurons. λ, $\lambda' = E, I$ label the excitation and inhibition; τ, σ_E, and σ_I denote the membrane, excitatory, and inhibitory timescales, respectively; V is the membrane potential; $G^{\lambda E}$ and $G^{\lambda I}$ are excitatory and inhibitory conductance, respectively, V_R, V_E, and V_I are the resting, excitatory, and inhibitory reversal potentials, respectively. The external input $\eta_{\alpha i}^{\lambda E} = \beta_{\alpha}^{E} f_E \Sigma_{\mu} \delta(t - T_{\alpha i}^{E\mu})$ uses a Poisson spike train $\{T_{\alpha i}^{E\mu}\}$ with strength f_E and a prescribed rate $\nu_{0E}(t)$. $\alpha = S, C$, labels simple and complex cells, respectively. Here, simple and complex cells are modeled by the following network architecture: $\beta_S^E = 1$, $\beta_C^E = 0$, i.e., simple cells are driven externally with excitatory inputs in addition to their inputs from other cells, whereas complex cells are not driven externally and receive inputs only from other cortical cells.¶ In our model, for the sake of presentation, half of the neurons are simple, the other half are complex, unless otherwise stated. $\gamma_{\alpha BD}^{\lambda\lambda'}$ are the inputs (feedback) to the neuron of type (λ, α) in the background from the neurons in the embedded subnetwork, which is symbolized by D.

Next, we replace these "background neurons" of Eq. **1** with a CG kinetic representation. As described in ref. 12, the CG kinetic theory studies the evolution of the probability density function: $\bar{\rho}_{\alpha}^{\lambda}(v, g_E, g_I; t) \equiv \mathbb{E}\,[(1/N_{\alpha}^{\lambda})\Sigma_{i=1}^{N_{\alpha}^{\lambda}}\{\delta[v - V_{\alpha i}^{\lambda}(t)]\delta[g_E - G_{\alpha i}^{\lambda E}(t)]\delta[g_I - G_{\alpha i}^{\lambda I}(t)]\}]$, where the expectation $\mathbb{E}$ is taken over all realizations of incoming Poisson spike trains $\{T_{\alpha i}^{E\mu}\}$, and over possible random initial conditions. N_{α}^{λ} is the number of neurons in the background population of (λ, α)-type. Define the marginal and conditional moments:

$$\rho_{\alpha}^{\lambda}(v; t) \equiv \int_0^{\infty} \bar{\rho}_{\alpha}^{\lambda}(v, g_E, g_I; t) dg_E dg_I,$$

$$\mu_{\alpha}^{\lambda E}(v; t) \equiv \int_0^{\infty} g_E \bar{\rho}_{\alpha}^{\lambda}(g_E, g_I|v; t) dg_E dg_I,$$

$$\mu_{\alpha}^{\lambda I}(v; t) \equiv \int_0^{\infty} g_I \bar{\rho}_{\alpha}^{\lambda}(g_E, g_I|v; t) dg_E dg_I,$$

where $\bar{\rho}_{\alpha}^{\lambda}(g_E, g_I|v; t)$ is the conditional probability density function, i.e., $\bar{\rho}_{\alpha}^{\lambda}(v_E, g_E, g_I; t) = \bar{\rho}_{\alpha}^{\lambda}(g_E, g_I|v; t)\ \rho_{\alpha}^{\lambda}(v; t)$. Upon closure assumptions (12), our CG kinetic theory of the dynamics (1) reduces to closed equations for $\rho_{\alpha}^{\lambda}(v; t)$, $\mu_{\alpha}^{\lambda E}(v; t)$, and $\mu_{\alpha}^{\lambda I}(v; t)$:

$$\partial_t \rho_{\alpha}^{\lambda} = \partial_v\{\zeta(v, \mu_{\alpha}^{\lambda E}, \mu_{\alpha}^{\lambda I})\rho_{\alpha}^{\lambda}\}, \quad [2a]$$

$$\partial_t \mu_{\alpha}^{\lambda E} = -\frac{1}{\sigma_E}(\mu_{\alpha}^{\lambda E} - \bar{g}_{\alpha}^{\lambda E}(t)) + \frac{\sigma_{\alpha}^{\lambda E^2}}{\tau \rho_{\alpha}^{\lambda}(v)} \partial_v[(v - V_E)\rho_{\alpha}^{\lambda}] + \zeta \partial_v \mu_{\alpha}^{\lambda E}, \quad [2b]$$

$$\partial_t \mu_{\alpha}^{\lambda I} = -\frac{1}{\sigma_I}(\mu_{\alpha}^{\lambda I} - \bar{g}_{\alpha}^{\lambda I}(t)) + \frac{\sigma_{\alpha}^{\lambda I^2}}{\tau \rho_{\alpha}^{\lambda}(v)} \partial_v[(v - V_I)\rho_{\alpha}^{\lambda}] + \zeta \partial_v \mu_{\alpha}^{\lambda I}, \quad [2c]$$

where $\zeta \equiv \zeta(v, \mu_{\alpha}^{\lambda E}, \mu_{\alpha}^{\lambda I}) \equiv \tau^{-1}[(v - V_R) + (v - V_E)\mu_{\alpha}^{\lambda E} + (v - V_I)\mu_{\alpha}^{\lambda I}]$ and

$$\bar{g}_{\alpha}^{\lambda\lambda'}(t) \equiv \beta_{\alpha}^{\lambda'} \nu_{0\lambda'}(t) f_{\lambda'} + S_{\alpha}^{\lambda\lambda'} \sum_{\alpha'} p m_{\alpha'}^{\lambda'}(t) + S_{\alpha BD}^{\lambda\lambda'} \sum_{\alpha'} p \tilde{m}_{\alpha'}^{\lambda'}(t), \quad [3a]$$

$$\sigma_{\alpha}^{\lambda\lambda'^2} \equiv \frac{1}{2\sigma_{\lambda'}}\left[\beta_{\alpha}^{\lambda'} f_{\lambda'}^2 \nu_{0\lambda'}(t) + (S_{\alpha}^{\lambda\lambda'})^2 \sum_{\alpha'} \frac{p m_{\alpha'}^{\lambda'}(t)}{N_{\alpha'}^{\lambda'}}\right] + \frac{(S_{\alpha BD}^{\lambda\lambda'})^2}{2\sigma_{\lambda'}} \sum_{\alpha'} \frac{p \tilde{m}_{\alpha'}^{\lambda'}(t)}{\tilde{N}_{\alpha'}^{\lambda'}}, \quad [3b]$$

where $\nu_{0\lambda'}(t)$ is the (temporally modulated) rate for the external Poisson spike train for λ'-population, and $m_{\alpha}^{\lambda}(t)$ is the average population firing rate per neuron of (λ, α)-type. $\tilde{m}_{\alpha}^{\lambda}(t)$ captures the feedback from the embedded point neurons (see *Supporting Text*, which is published on the PNAS web site). $\tilde{N}_{\alpha}^{\lambda}$ is the total number of embedded neurons of (λ, α)-type in the subnetwork. (Note that all the symbols with a tilde stand for the corresponding variables for the subnetwork of embedded point neurons.) $S_{\alpha}^{\lambda\lambda'}$ denotes the cortico-cortical synaptic connection strength from λ'-population to λ-population of α-cell type. $S_{\alpha BD}^{\lambda\lambda'}$ describes the coupling strength from the embedded subnetwork of λ'-population to the λ-population in the background. The stochastic nature of synaptic connection (17) is modeled by a Bernoulli random variable with release probability p (or synaptic failure probability $1 - p$). (For details, see *Supporting Text*.) These kinetic equations are posed for $V_I \le v \le V_T$, under two-point boundary conditions in v, which are derived from the fact that the total flux of neurons across firing threshold V_T is equal to the total flux at reset V_R (12), together with vanishing flux at $v = V_I$.

The dynamics of the remaining, i.e., the embedded, neurons is now described by

¶Note that, in this article, we merely use the terms "simple" and "complex" to refer to this particular network architecture. Neurons in the visual cortex are classified (16) "simple" or "complex," with simple cells responding to visual stimulation in an essentially linear fashion (for example, responding to sinusoidally modulated standing gratings at the fundamental frequency, with the magnitude of response sensitive to the spatial phase of the grating pattern), and with complex cells that respond nonlinearly (with a significant second harmonic) in a phase-insensitive manner. See refs. 14 and 15 for a model of simple and complex cells which captures these physiological features.

$$\tau \frac{d}{dt}\tilde{V}^{\lambda}_{\alpha i} = -(\tilde{V}^{\lambda}_{\alpha i} - V_R) - \tilde{G}^{\lambda E}_{\alpha i}(t)(\tilde{V}^{\lambda}_{\alpha i} - V_E) - \tilde{G}^{\lambda I}_{\alpha i}(t)(\tilde{V}^{\lambda}_{\alpha i} - V_I), \quad [4a]$$

$$\sigma_{\lambda'} \frac{d}{dt}\tilde{G}^{\lambda\lambda'}_{\alpha i} = -\tilde{G}^{\lambda\lambda'}_{\alpha i} + \tilde{\eta}^{\lambda\lambda'}_{\alpha i} + \tilde{\xi}^{\lambda\lambda'}_{\alpha i} + \gamma^{\lambda\lambda'}_{\alpha DB}, \quad [4b]$$

where $\tilde{\eta}^{\lambda\lambda'}_{\alpha i}$ and $\tilde{\xi}^{\lambda\lambda'}_{\alpha i}$ describe the external drive to the embedded neurons and their cortico-cortical couplings, respectively, and $\gamma^{\lambda\lambda'}_{\alpha DB} = S^{\lambda\lambda'}_{\alpha DB} \Sigma_{\alpha'} \Sigma_{\mu} \hat{p}^{\lambda'\mu}_{\alpha'} \delta(t - \hat{t}^{\lambda'\mu}_{\alpha'})$ describes the feedback from the CG populations to the embedded neurons (*Supporting Text*). Instead of using merely the average contribution to this feedback as described by the mean rate $pN^{\lambda}_{\alpha} m^{\lambda}_{\alpha}(t)$, we invoke the Poisson assumption and reconstruct stochastic spiking times $\{\hat{t}^{E\mu}_{\alpha}\}$ and $\{\hat{t}^{I\mu}_{\alpha}\}$ by using the total population rates $pN^{E}_{\alpha} m^{E}_{\alpha}(t)$ and $pN^{I}_{\alpha} m^{I}_{\alpha}(t)$ as the means for these Poisson spike trains, to capture spike fluctuations in our hybrid approach. Note that this Poisson spike reconstruction (PSR) automatically accounts for the spike fluctuation in the input via possibly sparse connections from the background, even if the number of neurons in the background is very large. We will demonstrate the significance of this PSR below.

Eqs. **2** and **4** constitute a network of point neurons (Eq. **4**) embedded within, and fully interacting with, a dynamical CG background represented by kinetic theory (Eq. **2**). The computation effort of this network involves only the simulation of a few embedded I&F neurons plus three (1 + 1)-D partial differential equations for simple and complex cells in the CG background. For statistical information, this approach allows us to drastically reduce computational cost otherwise needed in the simulation of the original, full I&F network (12) while retaining spike-timing information within the CG model.

Results

We have verified our hybrid approach by comparing the embedded network dynamics with the original full I&F network with the same underlying network architecture and parameters. First, we addressed accuracy and present an excellent comparison for systems in which different parts of the total network are replaced by the kinetic theory description.

Fig. 1 shows raster plots (spike times for each neuron) for five stimulus periods for a single CG patch containing 400 neurons. The raster plot for the full network of I&F neurons is shown in Fig. 1*a*, with the results for three embedded networks shown in Fig. 1 *b–d*. In these embedded networks, the eliminated point neurons are replaced by the kinetic theory CG background (Eq. **2**). Shown in Fig. 1 *b–d* are the spike rasters for the remaining, i.e., embedded I&F neurons, for comparison with the same neurons in the full network (Fig. 1*a*). In Fig. 1 *b* and *c*, respectively, half complex (simple) excitatory cells are described by the kinetic theory, whereas in Fig. 1*d*, half complex and half simple cells, again all excitatory, are described by the kinetic theory. Even in this case, the firing patterns of the embedded neurons (Fig. 1*d*) agree well with the full I&F network (Fig. 1*a*).

The networks shown in Fig. 1 are operating in a *fluctuation-dominant* regime (12). This regime can be a natural operating point for cortical networks (2, 18–20), whether there are external stimuli or not. The kinetic theory gives a valid, effective reduced description of such situations (12). Fig. 2 accentuates this point by comparing results for the same full network of 400 neurons as in Fig. 1, with those of the CG background represented by a CG mean firing-rate representation, $m^{\lambda}_{\alpha}(t)$, replacing kinetic theory. This mean firing-rate background is obtained by solving

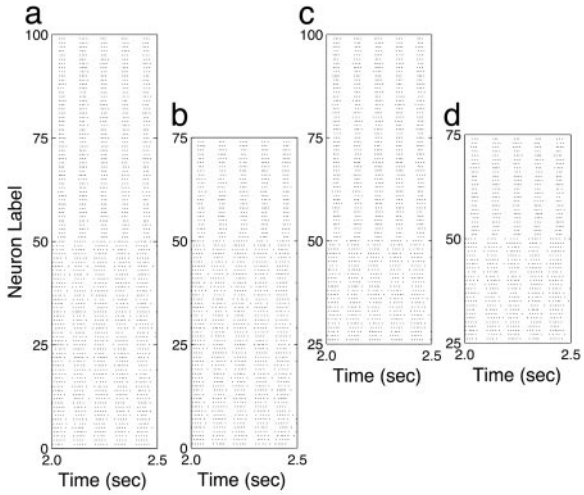

Fig. 1. Comparisons of raster plots of firing dynamics of the original I&F network, with networks with different components replaced by the kinetic theory description, for a single CG patch containing 400 neurons, 200 of which are simple (150 excitatory and 50 inhibitory) and 200 complex[¶] (150 excitatory and 50 inhibitory) with network connection probability $p = 0.25$. (The model networks in all figures always have 75% excitatory neurons and 25% inhibitory neurons.) External drive is modeled by Poisson-spike trains with the rate $f\nu_{0E}(t) = 20. \times (1 + 0.5 \sin(2\pi f_{\omega} t))$ with $f_{\omega} = 10$ Hz and $f = 0.01$, five stimulus periods are shown. Network parameters $\sigma_E = 5$ ms, $\sigma_I = 10$ ms, $V_R = -70$ mV, $V_T = -55$ mV, $V_E = 0$ mV, $V_I = -80$ mV (the same for all figures throughout) and $S_S = (S^{EE}_S, S^{EI}_S, S^{IE}_S, S^{II}_S) = (0.2, 0.4, 0.2, 0.4)$, and $S_C = (0.2, 0.4, 0.2, 0.4)$. [The order convention of $(S^{EE}, S^{EI}, S^{IE}, S^{II})$ will be used throughout.] Throughout, neurons indexed from 1 to 50 are *simple* excitatory, and neurons indexed from 51 to 100 are *complex* excitatory (inhibitory cells not shown). (*a*) The full network of I&F neurons. (*b*) Embedded networks with half of the complex cells coarse-grained. (*c*) Embedded network with half of the simple cells coarse-grained. (*d*) The embedded network with half of the simple and half of the complex cells coarse-grained. All CG populations are described by the kinetic theory (Eq. **2**) with PSR (see text).

$$m^{\lambda}_{\alpha}(t) = -\frac{\Gamma^{\lambda}_{\alpha}}{\log|1 - U^{\lambda}_{\alpha}(\{m^{\lambda'}_{\alpha'}\})|} \text{ for } U^{\lambda}_{\alpha} < 1; \quad m^{\lambda}_{\alpha}(t) \equiv 0, \text{ otherwise,} \quad [5]$$

for $\lambda, \lambda' = E, I$, $\alpha = S, C$, where $\Gamma^{\lambda}_{\alpha} = \tau^{-1}(1 + \bar{g}^{\lambda E}_{\alpha} + \bar{g}^{\lambda I}_{\alpha})$, $U^{\lambda}_{\alpha}(\{m^{\lambda'}_{\alpha'}\}) = ((V_T - V_R)/(V^{\lambda\alpha}_S - V_R))$, and $V^{\lambda\alpha}_S = \tau(\Gamma^{\lambda}_{\alpha})^{-1}(V_R + \bar{g}^{\lambda E}_{\alpha} V_E + \bar{g}^{\lambda I}_{\alpha} V_I)$, where $\bar{g}^{\lambda\lambda'}_{\alpha}$ are defined in Eq. **3a**. Eq. **5** can be derived (2) from the kinetic theory (Eq. **2**) by taking the limit $N \to \infty$, and $f_{\lambda} \to 0$, $f_{\lambda}\nu_{0\lambda}$ finite). Fig. 2 *b–d* clearly display the inaccuracy of the firing patterns of the remaining embedded neurons when compared with the same neurons in the full I&F network (Fig. 2*a*). In particular, note the complete failure of this mean firing-rate embedding (Fig. 2 *b–d*) to capture the firing of the complex cells in this fluctuation-driven case, whereas the kinetic theory embedding provides a faithful representation of the firing of these complex cells as shown in Fig. 1. Fig. 3 further corroborates this point. Shown are dynamic firing-rate curves for four representations in comparison with the full I&F network simulations of only simple cells. As clearly shown in Fig. 3, either purely mean-rate representation (as in the approach of ref. 11), or the hybrid approach using mean-rate only for the CG background, does not yield a quantitatively accurate description. We note that results, as shown in Figs. 1–3, can also be viewed as the validation of assumptions used in our CG kinetic theory. We will use only kinetic theory (Eq. **2**) below to describe the CG background, instead of Eq. **5**.

Our hybrid approach contains a distinct step of capturing the effects of fluctuations in the feedback to the embedded network

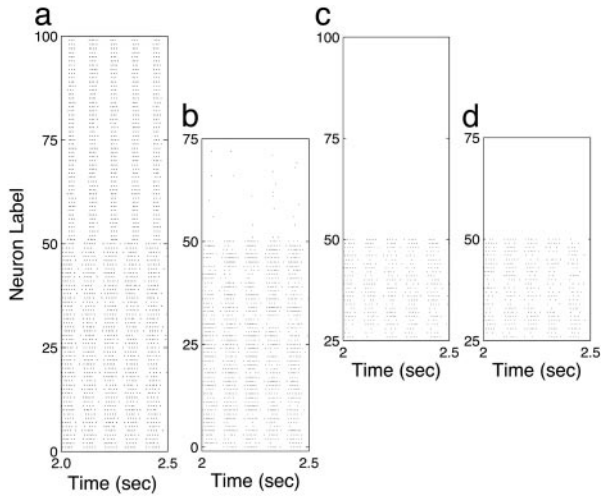

Fig. 2. Comparisons of raster plots of firing dynamics of the original I&F network with different components of the total network coarse-grained by the mean firing-rate description (Eq. **5**), for a single CG patch with the same network architecture and parameters as in Fig. 1. Throughout, neurons indexed from 1 to 50 are *simple* excitatory, and neurons indexed from 51 to 100 are *complex* excitatory (inhibitory cells not shown). (*a*) The full network of I&F neurons. (*b*) Embedded networks with half of the complex cells coarse-grained. (*c*) Embedded network with half of the simple cells coarse-grained. (*d*) The embedded network with half of the simple and half of the complex cells coarse-grained. All coarse-grained populations are described by Eq. **5**, rather than by kinetic theory (Eq. **2**).

from the CG background, which is accomplished by the Poisson-spike reconstruction as described above. Here, we contrast this step to a feedback of only the mean rate computed using the general kinetic theory (Eq. **2**) (*not* Eq. **5**!) without the PSR; i.e., $\gamma^{\lambda\lambda'}_{\alpha DB}$ is replaced by $S^{\lambda\lambda'}_{\alpha DB}\,\Sigma_{\alpha'}\,pN^{\lambda'}_{\alpha'}m^{\lambda'}_{\alpha'}(t)$ in Eq. **4b**. One might believe that a coupling of the kinetic theory to embedded-point

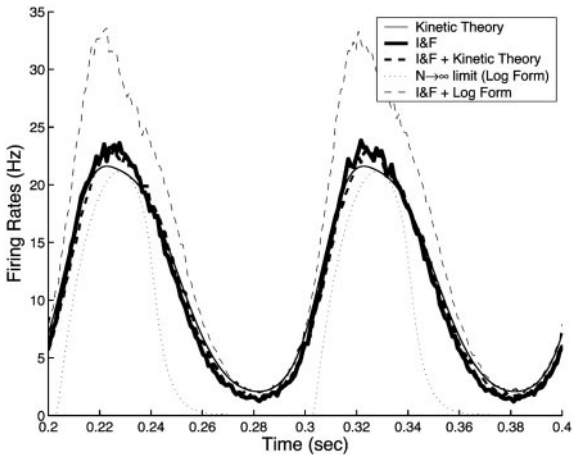

Fig. 3. Dynamic firing-rate curves for excitatory cells, for four representations in comparison with the full 400 I&F simple cell network simulations (thick solid line) with network connection probability $p = 0.25$. (*i*) All excitatory and inhibitory cells are coarse-grained using our kinetic theory (Eq. **2**) (thin solid line). (*ii*) All excitatory and inhibitory cells are coarse-grained using the mean firing-rate representation (Eq. **5**) (dotted line). (*iii*) All inhibitory cells are coarse-grained with the kinetic theory and the excitatory cells are modeled as embedded I&F neurons (thick dashed line). (*iv*) All inhibitory cells are coarse-grained using the mean firing-rate representation (Eq. **5**) and the excitatory cells are modeled as embedded I&F neurons (thin dashed line). The external drive is modeled by Poisson spike trains with the rate $f\nu_{0E}(t) = 13. \times (1 + 0.25\sin(2\pi f_\omega t)$, $f_\omega = 10$ Hz, and $f = 0.01$.

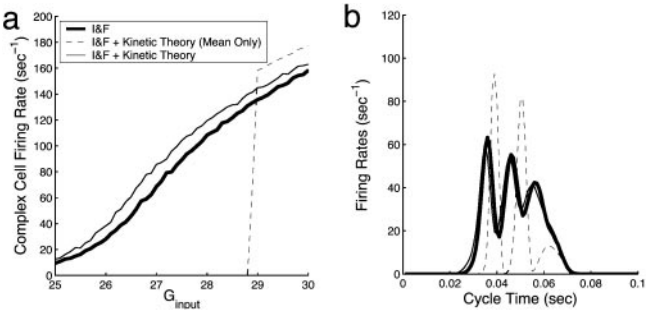

Fig. 4. Steady-state firing-rate curves as a function of the average input conductance (*a*) and cycle-averaged firing-rate curves for the embedded, excitatory complex cells¶ in a four-population model with both excitatory and inhibitory cells of simple and complex types in comparison with the full I&F simulations (thick solid line) of 400 neurons with network connection probability $p = 0.25$ (*b*). Half of the simple cells are coarse-grained using the kinetic theory (Eq. **2**) with the Poisson spike reconstruction in the feedback to the embedded point neurons (thin solid line), in contrast to where only the mean rate from the kinetic theory (Eq. **2**) is used in the feedback (dashed line). The external drive is modeled by Poisson spike trains with the rate $f\nu_{0E}(t) = 13. \times (1 + 0.5\sin(2\pi f_\omega t)$, $f_\omega = 10$ Hz and $f = 0.02$. Cycle-averaged firing rate is the rate averaged many periods of the stimulus at 10 Hz by $m(t) = \Sigma_{n=1}^{N_t} m(t + nT)/N_t$ for $0 < t < T$, where T is the period.

neurons through the direct use of this modulated mean firing rate would be just as effective. The results shown in Fig. 4 establish that it is not, i.e., it does not capture the fluctuations well enough for an accurate description. Fig. 4*a* shows firing-rate curves for excitatory complex neurons as a function of the average input conductance $G_{\text{input}} = f_E\nu_{0E}$ for steady inputs, whereas Fig. 4*b* shows cycle-averaged firing rate under temporally periodically modulated inputs. In both the steady state and dynamically modulated cases (Fig. 4), the firing rates of embedded neurons compare quantitatively very well with those of the full I&F network simulation when the PSR is used in combination of kinetic theory, whereas the modeling error in the rate of the embedded approach can be rather substantial without the proper fluctuation effect in the feedback from the CG background. Indeed, PSR is needed in fluctuation-dominated systems; thus, elsewhere in this article, we always use PSR.

Having addressed the modeling accuracy issues of the hybrid approach, we turn to the demonstration of its full power in modeling situations when there is a distinguished subnetwork of neurons which are sparse yet strongly coupled. Here, we consider an idealized network containing such a subnetwork, both to illustrate the necessity of the embedded network to model this situation efficiently and to contrast with another modeling situation in which "test neurons" within a kinetic theory can provide an adequate description.

The idealized network constitutes a four-population network of 400 neurons; each neuron is either simple or complex, excitatory or inhibitory. There are only eight complex cells in this network, forming a distinct subnetwork that is very strongly coupled. [Synaptic coupling strengths for these strongly coupled complex cells are $\tilde{S}_C = (0.4, 0.4, 0.8, 0.4)$ in contrast to $S_S = (0.1, 0.2, 0.1, 0.2)$ for the simple cells in the background and $S_{CDB} = (0.25, 0.2, 0.25, 0.2)$ and $S_{SBD} = (0.025, 0.05, 0.025, 0.05)$ for the couplings between the subnetwork and the CG background.] Fig. 5 displays the dynamics of this network characterized by (*i*) raster plots, (*ii*) cross-correlation as quantified by the conditional firing rate, i.e., the probability per unit time that the jth neuron fires, given the condition that the ith neuron fires, averaged over all i and j, and (*iii*) ISI distributions. These characteristics from the simulation of the full I&F network (*Lower*) are successfully reproduced by the hybrid approach (*Upper*), when all simple cells are coarse-grained using

NEUROSCIENCE

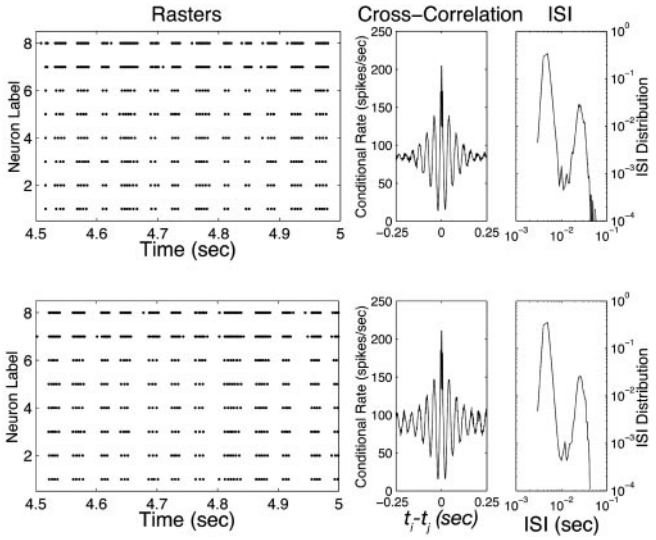

Fig. 5. Dynamics of strongly coupled embedded subnetwork on a background under an external input rate that is constant in time. Plotted are: (*i*) Raster plots, only the eight complex cells¶ in the distinct subpopulation are shown (neurons labeled 1–6 are excitatory, and those labeled 7–8 are inhibitory); (*ii*) cross-correlation (see text); and (*iii*) ISI distributions. (*Lower*) Simulation of the full I&F network; (*Upper*) Hybrid approach when all cells in the background are coarse-grained by using the kinetic theory, except for the eight distinct complex cells that are treated as an embedded network of point neurons.

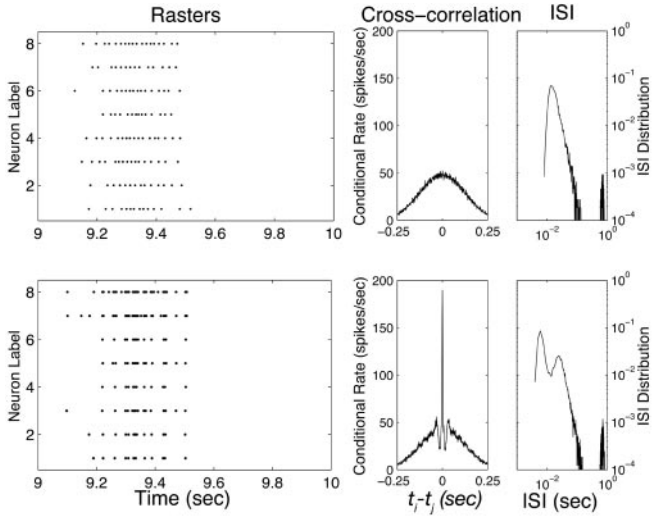

Fig. 6. Dynamics of strongly coupled embedded subnetwork on a background driven by a *time-dependent* stimulus. Plotted are: (*i*) Raster plots, only the eight complex cells¶ in the distinct subpopulation are shown (neurons labeled 1–6 are excitatory, and those labeled 7–8 are inhibitory); (*ii*) cross-correlation; and (*iii*) ISI distributions. (*Lower*) The hybrid approach when all cells in the background are coarse-grained by using the kinetic theory, and the eight distinct complex cells are treated as an embedded network of point neurons. (*Upper*) A subnetwork of eight *test neurons* in interaction with the background but without interaction among themselves. The external drive is modeled by Poisson spike trains with the rate $f\nu_{0E}(t) = 20. \times (1 + 0.25 \sin(2\pi f_\omega t)$, $f_\omega = 1$ Hz, and $f = 0.01$.

the kinetic theory, and the eight distinct neurons are treated as an embedded network of point neurons. These results demonstrate that our approach can successfully capture high-order statistics between two different neurons (e.g., cross-correlation) as well as for the same neuron (e.g., ISI). Instead of this constant external stimuli, a more useful and interesting situation for demonstrating the power of the hybrid approach is when the background actually has its own response dynamics to time-dependent stimuli. Here, the hybrid network really shows its ability to capture the distinct dynamics of the strongly interacting embedded subnetwork as demonstrated in the Fig. 6 *Lower*. Clearly, in addition to the cross-correlation induced by the external periodic drive (as captured by the test neurons in Fig. 6 *Upper*), the strongly interacting embedded neurons exhibit a stronger cross-correlation with more fine structure, which reflects relatively coherent recurrent dynamics of their own subnetwork. Furthermore, had we used merely test neurons to extract spike information of the embedded network, we would have obtained a singled-peaked ISI distribution instead of a double-peaked ISI distribution for the interacting embedded neurons (Fig. 6).

If one merely desires firing statistics of individual neurons *in the background*, test neurons in the embedded subnetwork will extract that information from a background whose full dynamics is modeled by kinetic theory. Fig. 7 shows excellent agreement between the ISI distribution of firing statistics of a sample neuron in a network, obtained by the full I&F network simulation, and that of a test neuron in the CG background description by kinetic theory.

To further illustrate the usefulness of the embedded neurons (actually in the sense of test neurons), we use our hybrid approach to construct a RTC (Fig. 8). RTC methods enable the experimentalist to probe the dynamical response of a cortical network from a system-analysis viewpoint. Based on "spike-triggered counting," these methods are most directly modeled by using detailed spike-timing information and thus are natural for the applications of embedded point-neuron networks. In one version of these methods (21), the experimentalist sequentially presents an anesthetized monkey with a grating stimulus, chosen randomly at every refresh time T_{refresh} from a collection of grating patterns with varying orientations and spatial phases, and measures the response of an individual cell in V1 extracellularly. For each spike, one asks at time τ earlier, what was the orientation and grating angle of the stimulus pattern presented? Running over all spikes, one measures the probability $P(\theta, \phi; \tau)$ that, at time τ before each spike, the stimulus had orientation θ and spatial phase ϕ. $P(\theta, \phi; \tau)$ provides an estimate of the first-order linear response function of the cortical system.

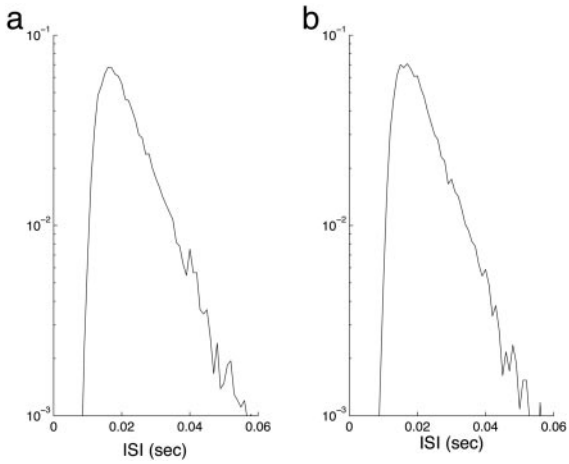

Fig. 7. Extraction of ISI distributions of neurons in the background, test neuron method. (*a*) Test neuron driven by a CG neuronal patch described by the kinetic theory. (*b*) Sample neuron from a full network of I&F neurons. We note that the firing rate of the neuron in the full I&F network is 46 spikes per sec, whereas the test neuron driven by the CG background has 45 spikes per sec, with only a 2% of relative error.

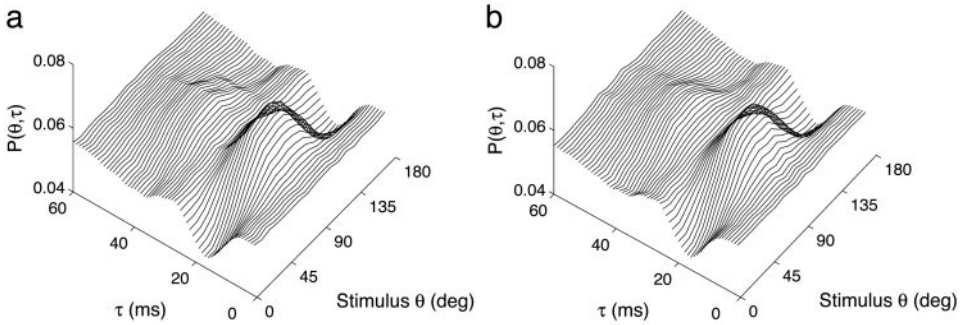

Fig. 8. Reverse-time correlation for a simple cell in a ring model for the orientation tuning dynamics of V1 neurons. (See *Supporting Text* for the LGN model we used.) The flash rate of the external patterns is 100 Hz. (*a*) RTC obtained from an I&F network simulation of the ring model. (*b*) RTC obtained by coarse-graining all complex cells in the ring model by using the kinetic equation.

We have constructed the RTC for neurons on a ring that models the orientation-tuning dynamics of V1 neurons (9, 12, 22, 23). The spatial (i.e., angular, here) couplings are described by Gaussian kernels. In the hybrid approach, the kinetic theory now has to be generalized to include multiple interacting angular populations to adequately model the orientation dynamics, and the coupling among these populations is the generalization of Eq. **3** (see *Supporting Text*). Fig. 8 shows phase-averaged $P(\theta, \tau) = \int P(\theta, \phi, \tau) d\phi$ for a representative simple excitatory cell, computed, respectively, from (*i*) a network of I&F neurons and (*ii*) an embedded network of point neurons within a CG background described by the kinetic theory. We obtain an excellent agreement between the result for the full I&F network with those of the embedded network.

Discussion

Computational modeling in visual neuroscience faces scale-up issues that must be resolved if the models are to represent regions of the visual cortex of sufficient size to capture the most interesting perceptual phenomena. For these purposes one must represent several cortical regions, each with multiple cortical layers of significant lateral extent, with their response potentially governed by fluctuations in conductances and voltages. The CG kinetic theory, such as developed in ref. 12, provides a possible resolution of these scale-up problems. However, these CG averaging techniques include a local averaging in time; hence, these methods do not retain detailed spike-timing information of the individual spiking neurons, information that may be needed for certain types of cortical processing.

Here, we have introduced an *embedded point-neuron representation*, benchmarked it for single CG patch, and applied it to an idealized ring model for orientation-tuning dynamics. This representation uses the advantages of the CG kinetic theory, while retaining detailed spike-timing statistical information for an embedded subnetwork of point neurons. We have shown that this embedded subnetwork approach is both numerically accurate and efficient. It has a wide range over which it can be implemented, from that of an individual "test neuron" to that of a distinguished subnetwork of sparse, strongly interacting point neurons, embedded within and fully interacting with the neuronal background described by a CG kinetic theory. We note that the main limitation to this CG approach arises when neurons fire with spike-to-spike synchrony in the background network.

This hybrid network approach can be very useful in a modeling situation in which the neurons in the network fall into distinct biological classes, say, one composed of neurons that are dense enough that averaging is natural; and the other class composed of neurons that are sparse (or have sparse synaptic connections), yet with their synapses strong enough that this sparse subnetwork fully interacts with the neurons of the other subnetwork. Biological possibilities for this sparse subnetwork include (*i*) neurons near positions of rapid change of cortical maps (such as near orientation pinwheel centers); (*ii*) neurons with long distance connections, which are relatively sparse, yet strong; (*iii*) neurons and synapses that describe connections between cortical layers; and (*iv*) neurons of some distinct anatomical type, with strong synapses. Where a strong sparse subnetwork is not present, kinetic theory can be used to represent the entire network, together with embedded "test neurons," which captures spike-timing statistical information, useful for modeling of certain important biological measurements, such as RTC.

Finally, another potential advantage of this embedded subnetwork approach is that the embedded neurons need not be I&F point neurons. Rather, more realistic models such as Hodgkin–Huxley compartmental models could be used without much loss of numerical efficiency (because of the relatively small number of neurons in the subnetwork).

This work was supported by a Sloan Fellowship and National Science Foundation Grants DMS-0211655 and DMS-0206679 (to D.C.), National Science Foundation Grant DMS-0211655 (to D.W.M.), and National Eye Institute Grant T32EY07158 (to L.T.).

1. Wilson, H. & Cowan, J. (1973) *Kybernetik* **13,** 55–80.
2. Shelley, M. & McLaughlin, D. (2002) *J. Comput. Neurosci.* **12,** 97–122.
3. Treves, A. (1993) *Network* **4,** 259–284.
4. Knight, B. (1972) *J. Gen. Physiol.* **59,** 734–766.
5. Abbott, L. & van Vreeswijk, C. (1993) *Phys. Rev. E Stat. Phys. Plasmas Fluids Relat. Interdiscip. Top.* **48,** 1483–1490.
6. Brunel, N. & Hakim, V. (1999) *Neural Comput.* **11,** 1621–1671.
7. Gerstner, W. (2000) *Neural Comput.* **12,** 43–80.
8. Sirovich, L., Omurtag, A. & Knight, B. (2000) *SIAM J. Appl. Math.* **60,** 2009–2028.
9. Nykamp, D. & Tranchina, D. (2000) *J. Comput. Neurosci.* **8,** 19–50.
10. Nykamp, D. & Tranchina, D. (2001) *Neural Comput.* **13,** 511–546.
11. Haskell, E., Nykamp, D. & Tranchina, D. (2001) *Network* **12,** 141–174.
12. Cai, D., Tao, L., Shelley, M. & Mclaughlin, D. (2004) *Proc. Natl. Acad. Sci. USA* **101,** 7757–7762.
13. McLaughlin, D., Shapley, R., Shelley, M. & Wielaard, J. (2000) *Proc. Natl. Acad. Sci. USA* **97,** 8087–8092.
14. Wielaard, J., Shelley, M., Shapley, R. & McLaughlin, D. (2001) *J. Neurosci.* **21,** 5203–5211.
15. Tao, L., Shelley, M., McLaughlin, D. & Shapley, R. (2004) *Proc. Natl. Acad. Sci. USA* **101,** 366–371.
16. Hubel, D. & Wiesel, T. (1962) *J. Physiol. (London)* **160,** 106–154.
17. Hardingham, N. R. & Larkman, A. U. (1998) *J. Physiol.* **507,** 249–256.
18. Stern, E., Kincaid, A. & Wilson, C. (1997) *J. Neurophysiol.* **77,** 1697–1715.
19. Anderson, J., Lampl, I., Gillespie, D. & Ferster, D. (2000) *Science* **290,** 1968–1972.
20. Fourcaud, N. & Brunel, N. (2002) *Neural Comput.* **14,** 2057–2110.
21. Ringach, D., Hawken, M. & Shapley, R. (1997) *Nature* **387,** 281–284.
22. Somers, D., Nelson, S. & Sur, M. (1995) *J. Neurosci.* **15,** 5448–5465.
23. Pugh, M., Ringach, D., Shapley, R. & Shelley, M. (2000) *J. Comput. Neurosci.* **8,** 143–159.